water

MDPI

Article

Spatial and Temporal Variations in Soil Salinity and Groundwater in the Downstream Yarkant River Irrigation District

Zhaotong Shen [1,2,†], Yungang Bai [3,*], Ming Zheng [2], Wantong Zhang [1,2,†], Biao Cao [2], Bangxin Ding [1], Jun Xiao [2] and Zhongping Chai [1,*]

[1] College of Resources and Environment, Xinjiang Agricultural University, Urumqi 830091, China; zhaotong_shen@163.com (Z.S.); 19981513393@163.com (W.Z.); dovebx@163.com (B.D.)
[2] Xinjiang Institute of Water Resources and Hydropower Research, Urumqi 830049, China; xjzhengming@126.com (M.Z.); xjskycb@sina.com (B.C.); 17699052619@163.com (J.X.)
[3] Xinjiang Ecological Water Resources Research Center, Urumqi 830099, China
* Correspondence: xjbaiyg@sina.com (Y.B.); chaizhongpingth@sina.com (Z.C.); Tel.: +86-138-9986-7569 (Y.B.); +86-135-6591-2598 (Z.C.)
† These authors contributed equally to this work.

Abstract

The downstream irrigation district of the Yarkant River basin has experienced increasing soil salinization driven by shallow groundwater levels, constraining the sustainable development of regional agriculture. However, the dynamic relationship between soil salinity and groundwater depth in this region remains unclear, limiting the effectiveness of saline–alkali land remediation strategies based on groundwater level regulation. In this study, field data were collected in 2025 on total soil salinity, concentrations of eight major ions, groundwater depth, and groundwater salinity in the irrigation district. The spatiotemporal distribution patterns of soil salinity, groundwater depth, and groundwater salinity were analyzed, along with their interrelationships. The soils in the irrigation district are predominantly mildly to moderately saline. Overall, soil salinity exhibits clear seasonal patterns, characterized by accumulation due to evaporation in spring and autumn and dilution through irrigation in summer. The dominant anions in the soil were SO_4^{2-} and Cl^-, while Ca^{2+} and Na^+ were the dominant cations, indicating a chloride–sulfate salinity type. Soil salinity shows a significant positive correlation with groundwater mineralization. A clear Boltzmann function relationship was identified between soil salinity and groundwater depth, revealing a critical groundwater depth of 2.10–2.18 m for salt accumulation in the irrigation district. The critical groundwater depths corresponding to soil salinity and major salt ions, from lowest to highest, are Cl^- < Na^+ < total salts < SO_4^{2-} < Ca^{2+}. Random forest regression analysis identified the main factors influencing soil salinity and their relative importance, ranked from highest to lowest as follows: groundwater depth > Na^+ > Cl^- > groundwater salinity > Ca^{2+} > SO_4^{2-} > Mg^{2+} > HCO_3^- > K^+ > CO_3^{2-}. Maintaining groundwater depth below the critical threshold and focusing on groundwater ions that strongly influence soil salinity can effectively alleviate soil salinization in the lower Yarkant River irrigation district caused by shallow, highly mineralized groundwater.

Keywords: soil salinization; groundwater; salt ions; degree of mineralization; spatiotemporal distribution

Check for updates

Academic Editor: Micòl Mastrocicco

Received: 25 November 2025
Revised: 16 December 2025
Accepted: 18 December 2025
Published: 19 December 2025

Copyright: © 2025 by the authors. Licensee MDPI, Basel, Switzerland. This article is an open access article distributed under the terms and conditions of the Creative Commons Attribution (CC BY) license.

1. Introduction

Soil salinization is a global ecological and environmental problem that poses a serious threat to sustainable agriculture and food security. Globally, saline–alkali soils account for approximately 10% of the total land area [1]. In China, these soils are widely distributed, covering about 5.01% of the country's arable land [2]. In the arid northwest region of China, intense evaporation and limited precipitation exacerbate both primary and secondary soil salinization. This process has led to the loss of large areas of arable land and has become a major constraint on the sustainable development of oasis agriculture [3]. Xinjiang, a key agricultural region in northwest China, is characterized by diverse types of saline–alkali soils, wide spatial distribution, and high degrees of salinization. Consequently, it has become a priority area for salinization research [4]. The Yarkant River Basin, located on the western margin of the Taklamakan Desert, is a representative region within this arid zone, where the downstream irrigation district experiences particularly severe soil salinization and secondary salinization.

Soil salinization is fundamentally a process of water–salt transport, commonly described by the principle that "salt moves with water and is removed with water" [5]. Therefore, clarifying the response mechanisms between groundwater dynamics and soil salinity is essential for developing effective and scientifically grounded management strategies. In recent years, extensive research has been conducted on water–salt transport processes. Guan et al. [6] applied GIS technology to analyze the spatiotemporal variability of soil salinity in the Shaohaoqu irrigation basin. Akramkhanov et al. [7] simulated the spatial distribution of soil salinity in intensively irrigated landscapes using environmental predictors. Jia et al. [8] developed a one-dimensional water–salt transport model under waterlogged infiltration conditions based on combined laboratory and field experiments. These studies mainly focused on the mechanisms and driving factors of water–salt migration, model simulation, and saline–alkali soil improvement. Most were conducted under artificially controlled conditions or based on single-point spatial data, emphasizing static characteristics or idealized scenarios. Consequently, the relationship between groundwater depth and soil salinity was not fully clarified, and few studies have examined seasonal variations in soil salinity and ion composition in the Yarkant River irrigation district. In many arid-region irrigation districts in China, groundwater distribution patterns resemble those of the Yarkant River irrigation district. Typically, groundwater in the upper and middle reaches is deep and weakly saline, whereas in downstream areas it is shallow and highly mineralized. This pattern mainly results from irrigation practices in downstream areas. Excessive irrigation infiltrates into the groundwater system and migrates downstream under gravity, reducing groundwater depth, enhancing water-table evaporation, and promoting salt accumulation in surface soils [9]. This process ultimately induces secondary soil salinization. In irrigation districts where salinization develops under such conditions, remediation measures based solely on physical, chemical, or biological approaches often fail to achieve sustainable outcomes. Effective management must therefore focus on regulating groundwater depth. Owing to its low topographic position, the downstream irrigation district of the Yarkant River is characterized by shallow groundwater levels and high groundwater mineralization.

Current research on the relationship between groundwater and soil salinity primarily focuses on the influence of groundwater depth. Cai Shijie [10] simulated groundwater dynamics in the Karamay irrigation district using the FEFLOW model. Tavakoli-Kivi et al. [11] applied a three-dimensional coupled model to simulate groundwater dynamics and soil salinity variations in an agricultural area of the Arkansas River Irrigation Valley in southeastern Colorado. Sahoo et al. [12] used machine learning algorithms combined with Kriging interpolation to predict spatial patterns of groundwater level changes. Although these studies highlight the role of groundwater depth in soil salinization, comprehensive

quantitative analyses of the interactions between soil salinity and groundwater remain limited. This gap restricts the ability to accurately tailor salinization prevention and control strategies to different soil types.

Random Forest is an ensemble machine learning algorithm that performs regression by constructing multiple decision trees and aggregating their predictions [13]. It is well suited for capturing complex nonlinear relationships [14] and enables assessment of feature importance. Lei et al. [15] applied several machine learning algorithms alongside physical models to predict soil salinity dynamics in farmland, showing that machine learning achieved accuracy comparable to, and in some cases exceeding, that of physical models. In another study, Random Forest combined with remote sensing data was used to identify an optimal assessment window for soil salinity in arid farmland [16]. Given the high predictive accuracy of Random Forest models in agricultural water–salt simulations, SHAP values derived from Random Forest regression can be used to quantitatively evaluate the influence of factors such as groundwater depth on soil salinity.

Based on this framework, this study focuses on the irrigation district in the lower reaches of the Yarkant River basin to investigate the spatiotemporal patterns of soil salinity variation. It analyzes the spatiotemporal evolution of groundwater depth and salinity, identifies the critical groundwater depth that triggers secondary salinization, and applies random forest regression to determine the primary factors controlling soil salinity in the irrigation district. This study provides a scientific basis for the precise prevention and control of soil salinization in irrigation districts and for the protection of ecological security.

2. Materials and Methods

2.1. Overview of the Study Area

The study area is located in Duolatibage Township, Bachu County (78°34′54″~78°39′17″ E, 39°46′09″~39°48′34″ N), and covers approximately 17.37 km^2 (Figure 1). It lies in the arid oasis zone on the northwestern margin of the Tarim Basin and has a temperate continental climate characterized by abundant sunshine and high light and heat availability. Precipitation is low and unevenly distributed throughout the year, with large diurnal temperature variations and frequent sandstorms and dust events. The area has an average elevation of 1115 m. Mean annual evaporation reaches 2350 mm, whereas mean annual precipitation is only 58 mm. The mean annual temperature is 11.8 °C. Soils in the irrigation district are classified as clay loamy (Table 1). The main crops are cotton and maize, which are irrigated by drip irrigation using water diverted from the Honghai Reservoir through the Qarbag Main Canal. The irrigation water has a mineralization degree of 0.6~1.0 g·L^{-1}. An artificial drainage channel runs along the eastern boundary of the study area, and the dominant irrigation regime in the district is winter–spring irrigation.

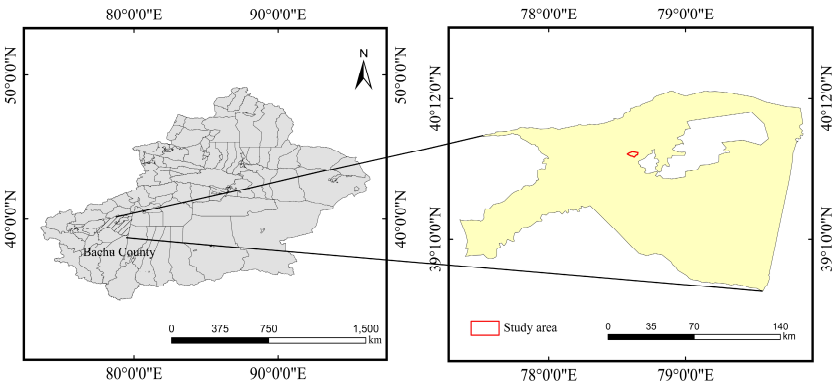


Figure 1. Location map of the study area.

Table 1. Soil texture in the study area.

Soil Depth (cm)	Clay (%)	Silt (%)	Sand (%)	Soil Texture
0~20	19.37	31.47	49.16	Clay loam
20~40	18.95	31.78	49.28	Clay loam
40~60	19.81	33.14	47.05	Clay loam
60~80	18.72	31.84	49.43	Clay loam
80~100	18.89	30.13	50.98	Clay loam

2.2. Sample Collection

Following the methodology of Zhao et al. [17], the study area was divided into a 1 km × 1 km grid. Soil sampling was conducted on 15 April, 15 July, and 15 October 2025, with sampling locations determined using GPS. A total of 30 sampling points were distributed across the study area, and soil samples were collected using soil augers (Figure 2). Layered sampling was carried out at depths of 0~20 cm, 20~40 cm, 40~60 cm, 60~80 cm, and 80~100 cm. At each sampling point, three replicate samples were collected at each depth, resulting in a total of 450 soil samples. All samples were placed in self-sealing bags, labeled, and stored under sealed conditions. For subsequent analysis, the mean value of the three replicates at each sampling point was used.

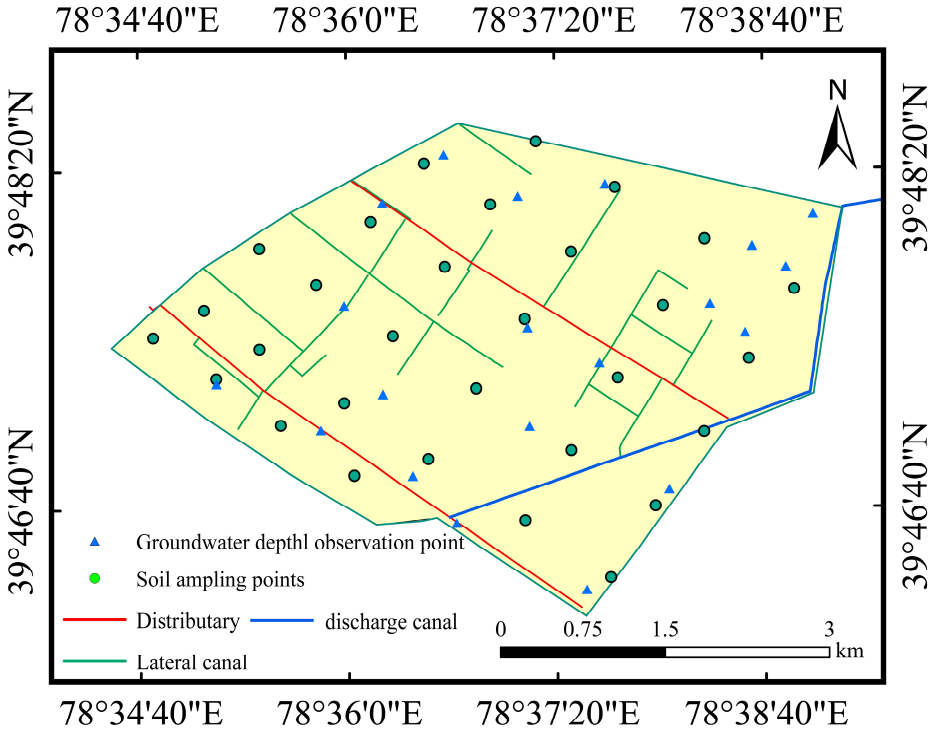


Figure 2. Schematic diagram of the sampling point location.

A total of 20 groundwater monitoring wells were installed in the study area. Groundwater depth measurements were conducted at all wells on 16 April, 16 July, and 16 October. Measurements were taken using a steel tape water level gauge (SWJ-80, Nanjing Xinsheng Hydrological Instrument Co., Ltd., Nanjing, China). Before measurement, the tape was cleaned, and the probe was slowly lowered into the well. When the probe contacted the water surface and emitted an audible signal, the depth at the point where the tape intersected the well rim was recorded. Each measurement was repeated three times, and the mean value was calculated. Groundwater depth was determined using the follow-

ing equation: Groundwater depth = measured depth − height from the well rim to the ground surface.

Groundwater sampling was conducted immediately after groundwater level measurement. A submersible pump (51A304, Xiaonengdou, Shangqiu, China) was placed into each monitoring well, and groundwater was pumped continuously at a low flow rate to the wellhead. Pumping was continued until parameters such as electrical conductivity stabilized for three consecutive measurements, with fluctuations less than 10%. The suction tube was then inserted to the bottom of the sampling bottle, and groundwater was slowly injected to avoid aeration. After the bottle was filled to two to three times its volume and overflowed, the cap was sealed tightly.

2.3. Measurements and Methods

2.3.1. Soil Sample Determination

Soil total salt content in April samples was determined using the dry residue method. For soil samples collected in July and October, salinity was measured by the electrical conductivity method (DDS-307; soil-to-water mass ratio of 1:5). SO_4^{2-} was determined by EDTA indirect titration, and Cl^- by $AgNO_3$ titration. K^+ and Na^+ were measured using atomic absorption spectroscopy. CO_3^{2-} and HCO_3^- were determined by the double-indicator neutralization method, while Ca^{2+} and Mg^{2+} were measured by EDTA complexometric titration [18].

2.3.2. Groundwater Sample Determination

The degree of mineralization of water samples was determined using the dry residue method. SO_4^{2-} was measured by EDTA indirect titration, and Cl^- by $AgNO_3$ titration. K^+ and Na^+ were analyzed using atomic absorption spectroscopy. CO_3^{2-} and HCO_3^- were determined by the double-indicator neutralization method, while Ca^{2+} and Mg^{2+} were measured by EDTA complexometric titration.

2.3.3. Random Forest Regression

Random Forest is an ensemble learning algorithm that constructs multiple decision trees and aggregates their predictions, achieving greater generalization ability and robustness than a single model. During node splitting in each tree, the algorithm does not evaluate all features. Instead, it randomly selects a subset of features, typically with a size equal to the square root of the total number of features, and identifies the optimal split within this subset. This strategy increases diversity among trees by ensuring that each tree captures different characteristics of the data. In this study, the Random Forest hyperparameters were set as follows: number of trees (n_estimators) = 100, maximum tree depth (max_depth) = 10, minimum samples required to split an internal node (min_samples_split) = 5, and minimum samples per leaf node (min_samples_leaf) = 2. A fixed random seed was used to ensure reproducibility. Because the objective was to identify the key factors influencing soil salinity through SHAP values rather than to evaluate predictive performance, the dataset was not divided into training and test sets. Instead, the entire dataset was used for model training.

2.4. Data Analysis

Data organization was carried out using Microsoft Excel 365. Spatial distribution maps of soil salinity, groundwater depth, and groundwater salinity were produced in ArcGIS 10.7 using Kriging spatial interpolation with a spherical model. Origin 2021 was used for graphical visualization, and Python 3.12 was employed for random forest regression analysis.

3. Results

3.1. Seasonal Statistics of Soil Salinity in the Irrigation District

Soil salinity in the study area exhibited pronounced seasonal variation (Table 2). In autumn, total soil salinity ranged from a minimum of 1.14 $g \cdot kg^{-1}$ to a maximum of 45.83 $g \cdot kg^{-1}$, indicating generally high salinity levels. According to the saline–alkali soil classification standards of Xinjiang, soils in the irrigation district are predominantly mildly to moderately saline–alkali, with some areas classified as severely saline–alkali. The coefficient of variation for total soil salinity ranged from 49.91% to 83.38%, reflecting uneven spatial distribution and moderate variability. The 0~20 cm soil layer consistently showed a high coefficient of variation across all seasons, indicating strong dispersion and complex spatial heterogeneity at this depth. Across the 0~80 cm soil profile, salinity was highest in autumn, lowest in summer, and intermediate in spring. Overall, soil salinity accumulated in spring and autumn due to evaporation and decreased during summer in response to irrigation.

Table 2. Statistical values of seasonal variations in soil salinity in Different soil layers.

Season	Soil Depth (cm)	Maximum ($g \cdot kg^{-1}$)	Minimum ($g \cdot kg^{-1}$)	Average ($g \cdot kg^{-1}$)	Standard Deviation	Coefficient of Variation %
spring	0~20	38.85	1.58	9.68	7.76	80.13
	20~40	19.31	1.56	7.65	4.58	59.86
	40~60	18.92	1.54	7.15	5.24	73.18
	60~80	14.71	1.41	5.95	3.64	61.2
	80~100	32.26	1.36	7.71	6.43	83.38
summer	0~20	32.96	2.09	10.95	7.94	72.49
	20~40	21.03	1.84	8.38	4.81	57.48
	40~60	17.87	1.23	6.27	4.99	79.73
	60~80	12.96	1.58	5.77	2.88	49.91
	80~100	15.45	1.67	6.13	4.02	65.55
autumn	0~20	45.83	1.40	11.65	9.55	82.03
	20~40	27.58	1.42	10.62	6.46	60.87
	40~60	22.82	1.14	7.22	5.08	70.44
	60~80	15.06	1.19	6.41	3.67	57.24
	80~100	15.49	1.26	6.70	3.48	52.01

3.2. Vertical Distribution Characteristics of Total Soil Salt and Salt Ions

Seasonal variations in soil salinity (Figure 3) indicate a strong influence of seasonal factors. Soil salinity in the 0~80 cm layer was significantly higher in autumn than in spring and summer. The 40~80 cm layer showed minimal seasonal variation, whereas the 0~40 cm and 80~100 cm layers exhibited pronounced seasonal fluctuations. Across all seasons, soil salinity in the 0~20 cm and 80~100 cm layers exceeded that of adjacent layers, indicating a clear surface accumulation pattern.

Based on the seasonal variation in soil salt ion concentrations (Figure 4), soils in the irrigation district contain relatively high levels of SO_4^{2-} and Cl^- among anions, and Ca^{2+} and Na^+ among cations, whereas K^+, Mg^{2+}, HCO_3^-, and other ions occur at lower concentrations. In spring, SO_4^{2-} and Cl^- concentrations ranged from 2.72 to 4.49 $g \cdot kg^{-1}$ and from 0.47 to 1.37 $g \cdot kg^{-1}$, respectively, while Ca^{2+} and Na^+ concentrations ranged from 0.70 to 1.58 $g \cdot kg^{-1}$ and from 0.44 to 1.12 $g \cdot kg^{-1}$. According to soil salinity classification criteria [19], the 0~40 cm soil layer in spring was classified as sulfate-salinized soil, whereas the deeper layers were classified as chloride–sulfate-salinized soil. Overall, chloride–sulfate-salinized soils predominate in the study area.

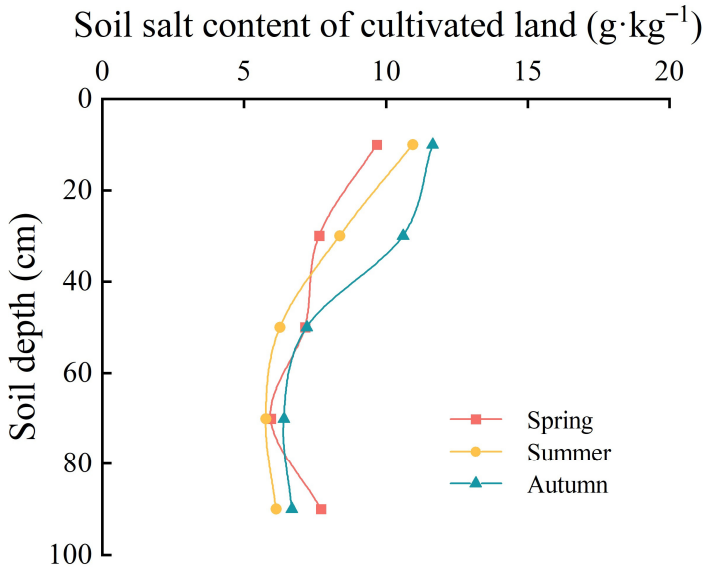


Figure 3. The variation in soil salt content in different seasons.

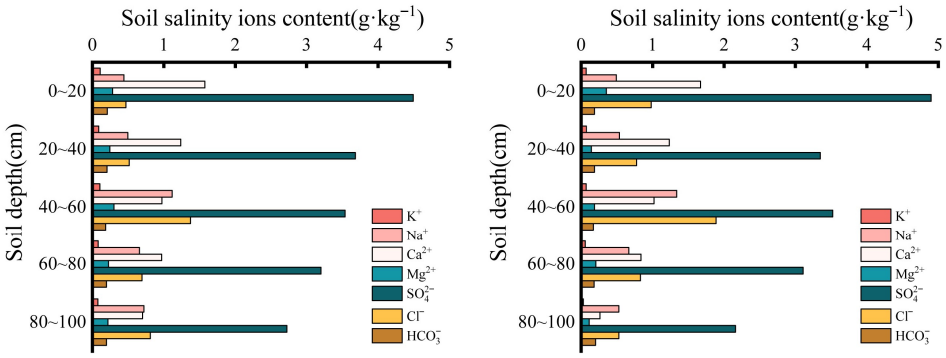


Figure 4. The content of soil salt ions in different seasons.

HCO_3^- concentrations remained relatively stable across all soil layers in both spring and autumn. In spring soils, SO_4^{2-} and Ca^{2+} concentrations gradually decreased with increasing depth, whereas Cl^- and Na^+ first increased and then decreased. K^+ and Mg^{2+} showed little variation among soil layers. In autumn soils, SO_4^{2-}, Cl^-, and Mg^{2+} concentrations varied markedly across layers but generally declined with depth. Na^+ concentrations initially increased and then decreased with depth, while Ca^{2+} exhibited an overall decreasing trend. K^+ remained relatively stable with only minor fluctuations. Soil salt ion concentrations are slightly lower in spring than in autumn, indicating that evaporation–leaching processes influence their distribution.

3.3. Spatiotemporal Distribution Characteristics of Soil Salinity

Seasonal soil salinity interpolation maps (Figure 5) show clear spatial heterogeneity, with values ranging from 1.14 to 45.83 g·kg^{-1}. Soil salinity was highest in autumn and lowest in summer, while spring values were slightly lower than those in autumn. Across all seasons, salinity was consistently higher in surface soils than in deeper layers, indicating a clear surface accumulation pattern. Spatial patterns were broadly consistent among seasons. Persistent high-salinity zones were concentrated in the northeastern and southeastern parts of the study area, where surface salinity reached up to 38.85 g·kg^{-1}. In contrast, the western, northwestern, and central regions maintained relatively low salinity levels, generally around 3 g·kg^{-1}. In summer, areas with surface salinity exceeding 10 g·kg^{-1} were mainly confined to the eastern and southeastern regions, whereas salinity in the

middle and deeper soil layers remained low throughout the area. Overall, soil salinity decreased gradually from east to west across seasons, demonstrating stable spatial hotspots despite seasonal variation.

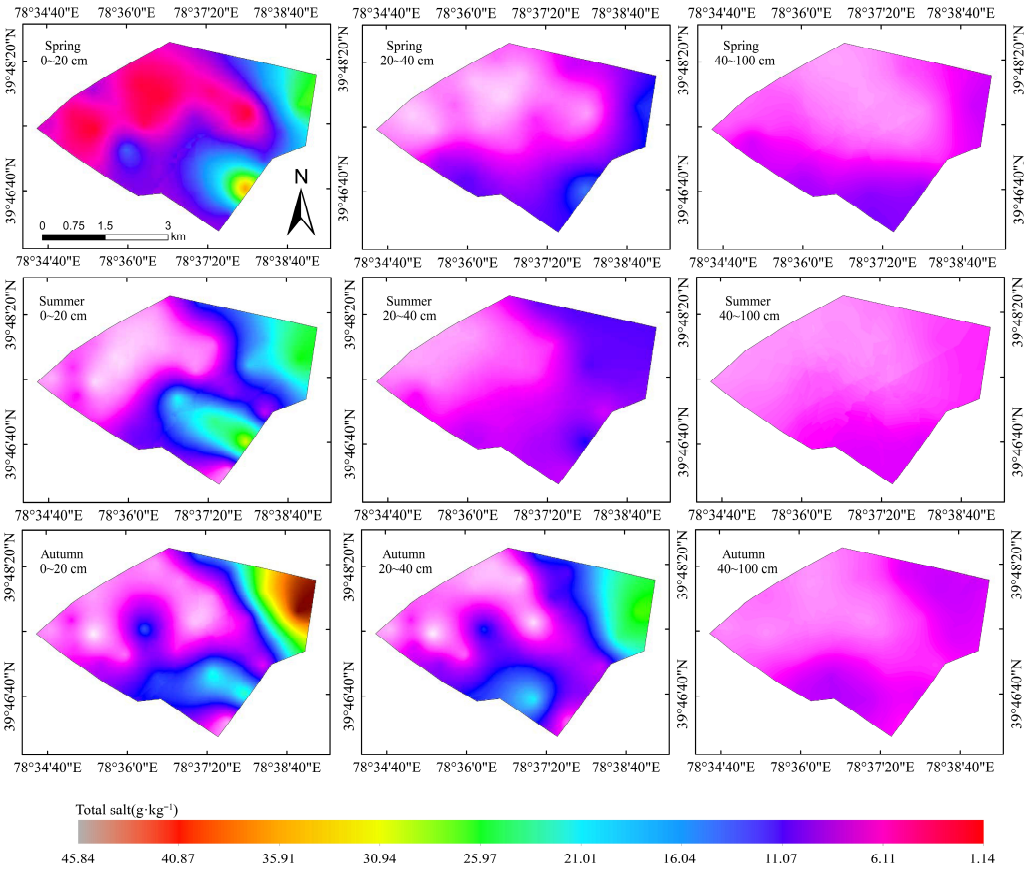


Figure 5. Spatial distribution of soil salinity in different soil layers in different seasons.

3.4. Salinity Composition and Correlation Between Soil and Groundwater in the Irrigation District

Piper diagrams were constructed using milliequivalent percentages of spring soil and groundwater ions, based on 15 randomly selected sampling points each (Figure 6a for soil and Figure 6b for groundwater). In the soil diagram (Figure 6a), cations mainly cluster in the lower triangular field, with $K^+ + Na^+$ and Ca^{2+} showing relatively high proportions, while Mg^{2+} contributes less. Anions are concentrated in the upper triangular field, where SO_4^{2-} accounts for a much higher proportion than Cl^- and $CO_3^{2-} + HCO_3^-$, indicating sulfate-dominated soil salinity. In the groundwater diagram (Figure 6b), $K^+ + Na^+$ also dominate the cations, whereas SO_4^{2-} and Cl^- are the dominant anions. Overall, both soil and groundwater chemistry are characterized by high proportions of $K^+ + Na^+$, Ca^{2+}, SO_4^{2-}, and Cl^-. The overlapping distributions of soil and groundwater samples indicate similar hydrochemical facies, suggesting a common ionic origin. This consistency implies ongoing salt exchange between soil and groundwater systems, likely driven by irrigation infiltration and evaporation processes.

Correlation analysis of soil and groundwater ions was performed using data from 15 randomly selected sites in each season (Figure 7). Groundwater salinity showed extremely significant positive correlations ($p < 0.01$) with K^+(G), Na^+(G), Ca^{2+}(G), Mg^{2+}(G), SO_4^{2-}(G), Cl^-(G), and CO_3^{2-}(G). Total soil salt content was highly significantly positively correlated with Na^+(S), Ca^{2+}(S), Mg^{2+}(S), SO_4^{2-}(S), and Cl^-(S). Total soil salinity also exhibited significant positive correlations ($p < 0.05$) with Na^+(G), Ca^{2+}(G), Mg^{2+}(G), SO_4^{2-}(G), Cl^-(G), and groundwater mineralization. In addition, Na^+(S) was significantly

positively correlated with Na^+(G), Ca^{2+}(S) with Ca^{2+}(G), Mg^{2+}(S) with Mg^{2+}(G), SO_4^{2-}(S) with SO_4^{2-}(G), and Cl^-(S) with Cl^-(G) ($p < 0.05$). Overall, soil salinity showed a significant positive relationship with groundwater mineralization, and major soil ions were strongly correlated with their corresponding groundwater ions. These results indicate active salt exchange between soil and groundwater systems, driven by irrigation, evaporation, and related processes.

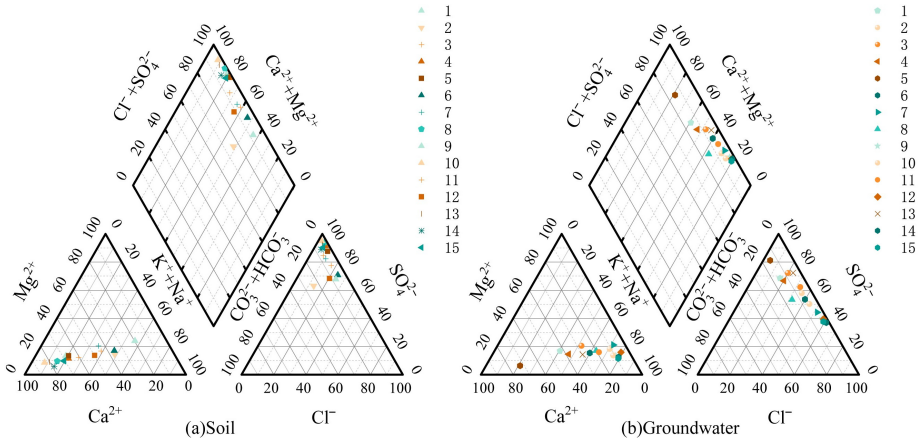


Figure 6. Spring groundwater and soil salt ion Piper trilinear diagram.

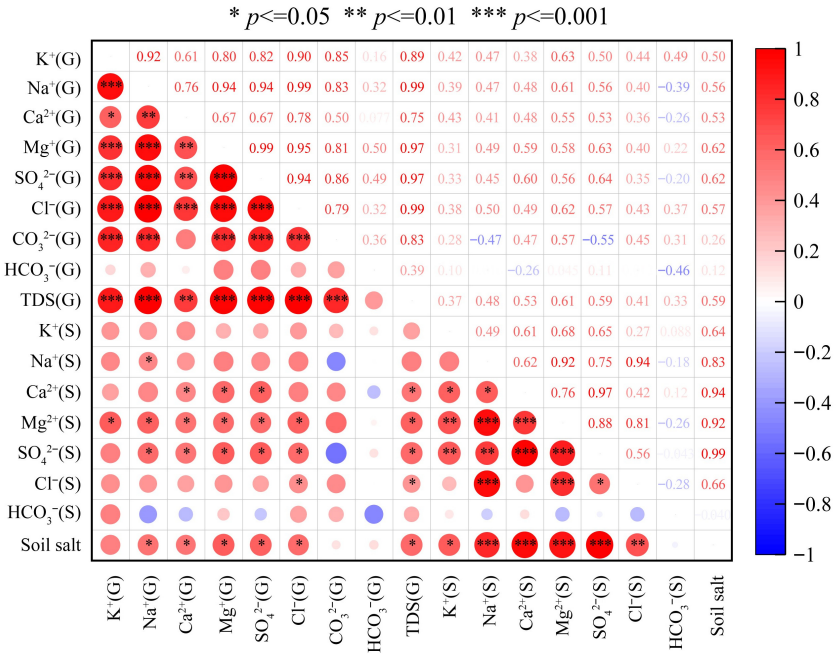


Figure 7. Correlation analysis of salt ions in soil and groundwater. Note: The ion suffix (G) indicates that the ion is an ion in groundwater. (S) indicates that the ion is an ion in the soil; TDS stands for the mineralization degree of groundwater. Soil salt refers to total soil salt content.

3.5. Spatiotemporal Distribution Characteristics of Groundwater Depth and Mineralization

The seasonal spatial distribution of groundwater depth is illustrated in Figure 8. Groundwater depth shows pronounced spatial variability across the irrigation district. Deeper groundwater levels (>2 m) are mainly found in the northern and central-eastern parts of the study area, whereas shallower depths (<2 m) occur primarily in the north-eastern, southern, and western regions. Overall, groundwater is relatively shallow in the southern, northern, and central areas, with depth increasing gradually toward the east and west. Areas with shallow groundwater generally overlap with zones of high soil salinity

(Figures 5 and 8). In spring, minimum groundwater depths were less than 1 m, posing a serious constraint on crop growth. Mean groundwater depths in spring, summer, and autumn were 1.20 m, 2.15 m, and 2.26 m, respectively, indicating a seasonal deepening trend from spring to autumn.

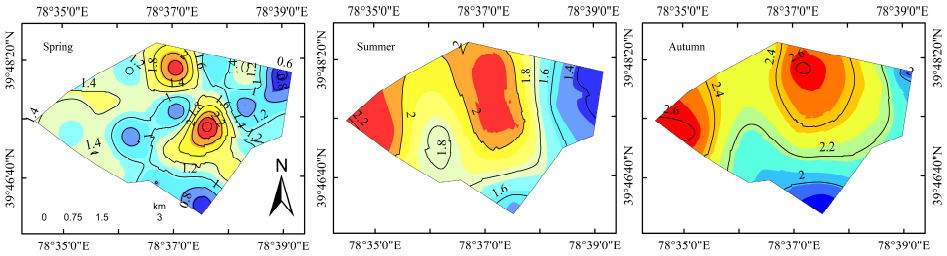


Figure 8. Spatial distribution of groundwater burial depth in different seasons.

The seasonal spatial distribution of groundwater mineralization is presented in Figure 9. Higher mineralization levels are mainly observed in the eastern and southern parts of the study area, reaching approximately 20 $g \cdot L^{-1}$, whereas lower mineralization levels (<16 $g \cdot L^{-1}$) are concentrated in the western region. Overall, groundwater mineralization exhibits no pronounced seasonal variation. During the winter and spring irrigation periods, large irrigation volumes combined with insufficient drainage lead to shallow groundwater levels in spring. As summer progresses, evaporation intensifies, promoting upward groundwater movement. Under strong evaporative conditions, salt ions are transported from groundwater into the soil through capillary rise and evaporation, resulting in increased soil salinity.

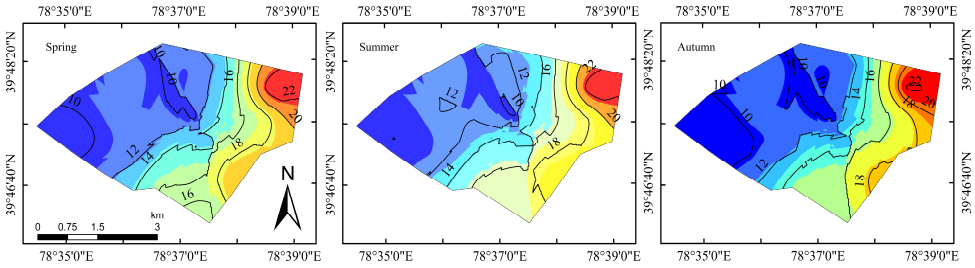


Figure 9. Spatial distribution of groundwater mineralization degree in different seasons.

3.6. Determination of the Critical Groundwater Depth in the Irrigation District

The inflection point of the Boltzmann curve represents the critical groundwater depth at which the influence of groundwater on surface soil salinity begins to weaken [20,21]. Soil salinity in the 0–40 cm and 0–100 cm layers was fitted to groundwater depth and mineralization using the Boltzmann function (Figure 10a). The coefficients of determination for the relationships between soil salinity and groundwater depth were 0.78 for the 0–40 cm layer and 0.73 for the 0–100 cm layer, indicating a good fit. The correlation with groundwater depth was stronger in the topsoil than in the entire soil profile. The inflection point of the fitted curve represents the groundwater depth at which its influence on surface soil salinity begins to weaken. When groundwater is shallower than this critical depth, capillary rise transports salts toward the surface, resulting in increased soil salinity. When groundwater depth exceeds this threshold, capillary effects diminish and soil salinity decreases. As shown in Figure 10a, the critical groundwater depths are 2.10 m for the topsoil (0~40 cm; 95% confidence interval: 2.00~2.21 m) and 2.18 m for the entire soil profile (0~100 cm; 95% confidence interval: 2.09~2.27 m). In contrast, Figure 10d shows a weak relationship between soil salinity and groundwater salinity, with no clear linear correlation.

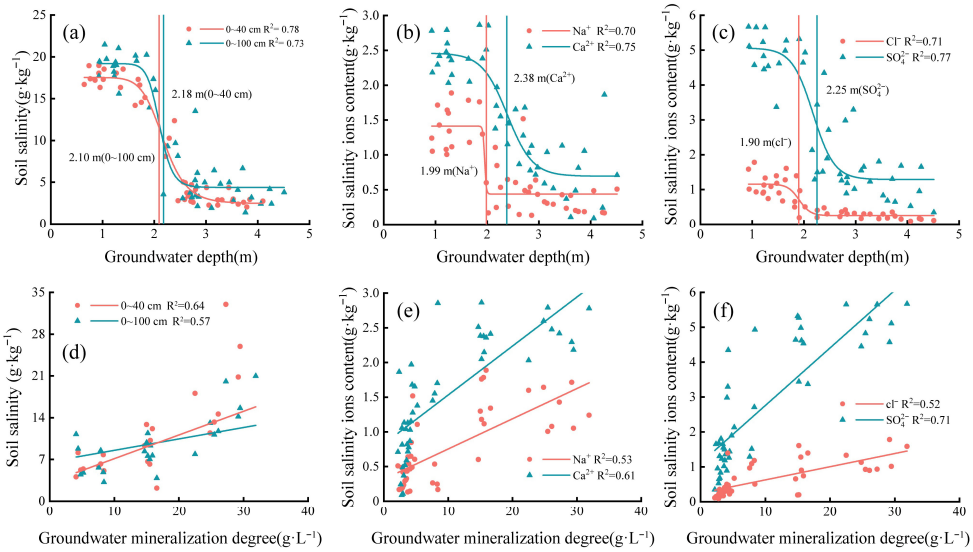


Figure 10. The fitting relationship between groundwater depth and soil salinity. Note: (**a**) Fitted relationships between soil salinity in the 0–40 cm and 0–100 cm depth layers and groundwater depth; (**b**) Fitted relationships between major soil cations and groundwater depth; (**c**) Fitted relationships between major soil anions and groundwater depth; (**d**) Fitted relationship between soil salinity in the 0–40 cm and 0–100 cm depth layers and groundwater mineralization degree; (**e**) Fitted relationship between major soil cations and groundwater mineralization degree; (**f**) Fitted relationship between major soil anions and groundwater mineralization degree. TDS stands for the mineralization degree of groundwater.

Figure 10b,c illustrate the relationships between major soil salt ions and groundwater burial depth. The coefficients of determination for Na^+, Ca^{2+}, SO_4^{2-}, and Cl^- were 0.70, 0.75, 0.77, and 0.71, respectively, indicating strong fits and clear functional relationships with groundwater depth. The critical burial depths were estimated as 1.99 m for Na^+ (95% confidence interval: 1.90~2.08 m), 2.38 m for Ca^{2+} (95% confidence interval: 2.20~2.58 m), 2.25 m for SO_4^{2-} (95% confidence interval: 2.09~2.34 m), and 1.90 m for Cl^- (95% confidence interval: 1.78~2.03 m). Accordingly, the groundwater critical burial depths for total soil salinity and major ions increased in the order $Cl^- < Na^+ <$ total salts $< SO_4^{2-} < Ca^{2+}$. These differences primarily reflect variations in ion migration rates within the soil and exchange processes between soil and groundwater. As shown in Figure 10e,f, among the major ions, only SO_4^{2-} shows a clear linear relationship with groundwater salinity ($R^2 = 0.71$), whereas the other ions exhibit weaker correlations.

3.7. Determination of the Main Controlling Factors of Soil Salinization in the Irrigation District

A random forest model was used to identify the primary factors influencing soil salinity. Groundwater depth, groundwater salinity, and groundwater ion concentrations were included as input variables, with soil salinity as the response variable. Because the objective was factor interpretation rather than prediction, model performance on a test set was not required. Accordingly, the entire dataset was used for model training, and no training–test split was applied. Model reliability was evaluated using the coefficient of determination (R^2) on the training data.

Random forest regression was used to assess the effects of groundwater depth, groundwater mineralization, and groundwater ions on soil salinity, yielding high fitting accuracy ($R^2 = 0.88$). SHAP analysis (Figure 11) shows that groundwater depth has the highest importance, making it the dominant control on soil salinity. The next most influential factors are groundwater Na^+ and Cl^-, while groundwater mineralization has a slightly weaker effect than Cl^-. The SHAP values for Ca^{2+} and SO_4^{2-} exhibit similar distributions,

indicating comparable influences on soil salinity, with Ca^{2+} having a marginally stronger effect. In contrast, Mg^{2+}, HCO_3^-, K^+, and CO_3^{2-} display SHAP values clustered near zero, suggesting that these ions exert relatively minor influences on soil salinity within the study area.

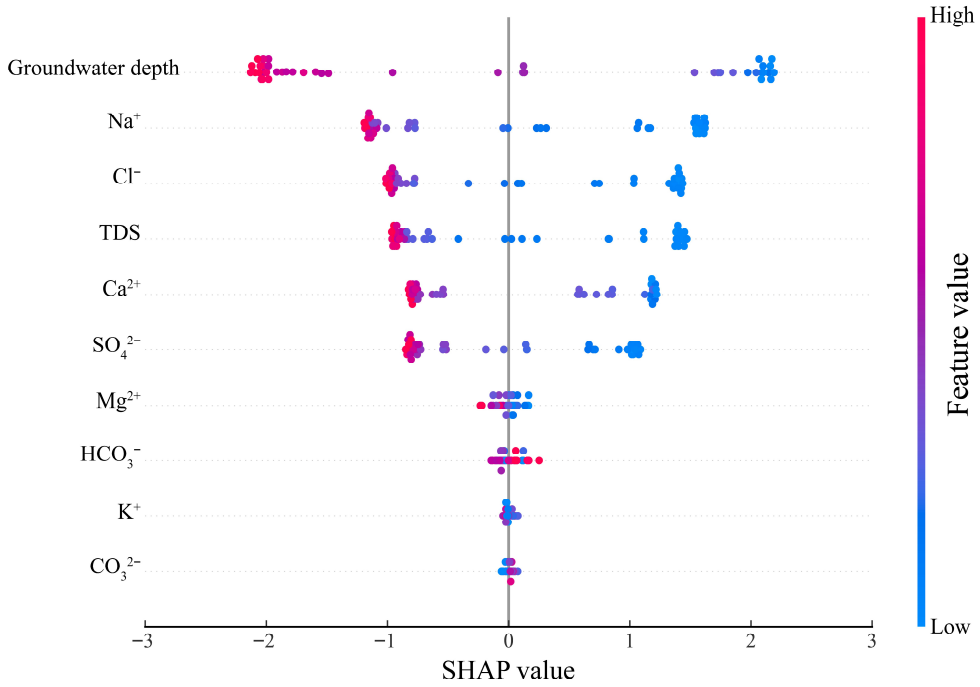


Figure 11. Importance of SHAP Features. Note: TDS stands for the mineralization degree of groundwater.

4. Discussion

4.1. Spatiotemporal Distribution Characteristics of Soil Salinity and Their Causes in the Irrigation District

This study shows that soil salinity in the irrigation district follows a clear seasonal pattern characterized by "autumn accumulation, summer depletion, and spring transition." Soil salinity reaches its annual minimum in summer, likely due to peak crop growth and intensive irrigation, during which infiltrating irrigation water effectively leaches and dilutes salts within the soil profile [22]. Soluble salts are dissolved by irrigation water or precipitation and transported downward through soil pores to deeper layers or beyond the root zone, resulting in soil desalination [23]. Previous studies have reported a marked decrease in surface soil salinity (0–60 cm) after irrigation, whereas salinity in deeper layers remains unchanged or increases slightly, further supporting the downward migration of salts [24]. Similar patterns have been observed in the Weigan River oasis [25]. In autumn, crop harvest is often accompanied by reduced or discontinued irrigation. Enhanced surface evaporation and decreased crop transpiration promote upward capillary movement of groundwater salts, leading to continuous salt accumulation and the formation of a pronounced "autumn salinity peak," particularly in arid and semi-arid regions [26]. In spring, overall soil salinity is lower than in autumn due to snowmelt and spring irrigation; however, an early-stage accumulation trend is already evident, indicating the onset of seasonal salt return processes [27]. Vertically, soil salinity in all seasons exhibits a surface accumulation pattern, with higher salinity concentrated in the 0–20 cm layer. The relatively high coefficient of variation in this layer may be associated with irrigation practices or tillage operations [28]. These results suggest that soil salinity dynamics in the study area are controlled not only by surface evaporation but also by groundwater fluctuations and soil texture stratification. Surface salinity predominantly results from upward migration

under strong evaporative conditions, whereas subsurface salt accumulation is likely related to seasonal groundwater level variations and restricted vertical migration caused by low-permeability layers [29,30].

4.2. Spatiotemporal Distribution Patterns of Groundwater Depth, Soil Salinity, and Mineralization and Their Interrelationships

This study indicates that groundwater burial depth in the irrigation district shows clear seasonal variation, with mean depths of 1.20 m in spring, 2.15 m in summer, and 2.26 m in autumn. These variations are mainly driven by irrigation practices, topography, and climatic conditions [31]. The observed pattern differs from that reported by Cai et al. [27], likely because the lower Yarkant River irrigation district primarily adopts a winter–spring irrigation regime. In spring, large inputs from snowmelt and spring irrigation, combined with insufficient drainage in some areas, cause groundwater levels to rise, with minimum burial depths falling below 1 m. Despite being the peak irrigation season, groundwater burial depth increased in summer due to strong crop transpiration, enhanced surface evaporation, and improved drainage conditions in parts of the area. After crop harvest in autumn, the cessation of irrigation reduced groundwater recharge, leading to further deepening of the groundwater table. This pattern is consistent with the findings of Wang et al. [32].

This study clarifies the intrinsic mechanisms governing soil salinity evolution in irrigated areas from the perspective of water–salt transport. Soil salt composition is dominated by SO_4^{2-} and Cl^- as major anions and by Ca^{2+} and Na^+ as principal cations, classifying the soils as chloride–sulfate type. This pattern is closely associated with the surface accumulation of soluble salts under strong evaporative conditions in arid regions [33]. Spring snowmelt infiltration and leaching cause Cl^- and Na^+ to exhibit migration patterns characterized by initial increases followed by decreases, reflecting their high solubility and mobility in soil pore water. This behavior mainly results from differences in ion adsorption–desorption processes and interactions with soil colloids [34]. In autumn, intense evaporation enhances upward soil moisture movement and drives salts from deeper layers toward the surface along water potential gradients [35]. The similarity in soil and groundwater ion compositions revealed by Piper diagrams, together with significant correlations between corresponding soil and groundwater ions, further demonstrates their close linkage. During periods of strong evaporative concentration, groundwater rises via capillary action while transporting dissolved salts into the soil profile, forming a continuous water–salt exchange pathway. These findings provide a theoretical basis for improving understanding of soil salinization processes in arid irrigated soils.

4.3. Main Controlling Factors of Soil Salinization in the Irrigation District

Theoretical studies on soil water–salt transport constitute a core component of saline–alkali soil research [36]. This study quantitatively demonstrates a significant functional relationship between soil salinity and groundwater depth. The coefficients of determination (R^2) for the fitted relationships reached 0.78 for the topsoil (0~40 cm) and 0.73 for the entire soil profile (0~100 cm), confirming a strong linkage between groundwater depth variations and soil salinity dynamics. Chen Yongbao et al. [37] reported that capillary action intensifies markedly when groundwater depth is shallower than 2.10 m, whereas beyond this threshold its strength decreases by approximately 70%, leading to a dynamic equilibrium in salt transport. These findings are consistent with the results of the present study. In addition, clear functional relationships were identified between major soil salt ions and groundwater depth, although the critical depths differed slightly from that of total soil salinity. The critical groundwater depth increased in the order Cl^- < Na^+ < total salts < SO_4^{2-} < Ca^{2+}. This pattern mainly

reflects differences in ion migration velocities and soil–groundwater ion exchange processes, in agreement with the conclusions of Qi et al. [38].

Sun et al. [39] demonstrated strong performance of decision tree regression in analyzing relationships between soil salinity and environmental factors. Amaranto et al. [40] applied multiple machine learning algorithms, including random forest, to accurately predict groundwater depth variations in agricultural fields. Building on this work, the present study employs random forest regression to explore the complex relationship between groundwater conditions and soil salinity. The model achieved high accuracy (R^2 = 0.88), and SHAP analysis identified groundwater depth, groundwater Na^+, Cl^-, and groundwater salinity as the dominant controls on soil salinity. The relative importance of influencing factors decreased in the following order: groundwater depth > Na^+ > Cl^- > groundwater salinity > Ca^{2+} > $SO_4{}^{2-}$ > Mg^{2+} > $HCO_3{}^-$ > K^+ > $CO_3{}^{2-}$.

The results indicate that the critical groundwater depth triggering soil salinization ranges from 2.10 to 2.18 m. This range is consistent with the 1.70–2.30 m threshold reported by Wang Guoshuai et al. [41] for the Hetao Irrigation District, supporting its broader applicability to water–salt management in arid irrigated regions. These findings provide a scientific basis for precise groundwater regulation, as maintaining groundwater depth above the critical threshold can reduce soil salinization risk by 35–50%, thereby contributing to regional agricultural sustainability. Although this study clarifies the response of soil salinity to groundwater depth based on field observations, some limitations remain. Future research should integrate soil physical properties, high-frequency monitoring data, and numerical simulations of water–salt transport to develop a comprehensive model that accounts for the combined effects of multiple controlling factors. Such efforts would further improve the prediction, management, and mitigation of soil salinization in irrigation districts.

5. Conclusions

Soil salinity in the irrigation district ranged from 1.14 to 45.83 g·kg^{-1}, with soils predominantly classified as mildly to moderately saline. Salinity displayed pronounced seasonal variation, following the pattern autumn > spring > summer. Salt accumulation occurred mainly in spring and autumn due to evaporation, whereas summer irrigation promoted salt leaching and reduced soil salinity. The dominant anions in saline soils were $SO_4{}^{2-}$ and Cl^-, and the primary cations were Ca^{2+} and Na^+. Accordingly, soils were mainly classified as chloride–sulfate saline–alkali, with clear seasonal fluctuations in ion concentrations. Soil salinity showed a strong functional relationship with groundwater depth, and the critical depth for salt accumulation ranged from 2.10 to 2.18 m. Maintaining groundwater depth above 2.18 m can effectively suppress soil salinization in the irrigation district. The critical groundwater depths for total soil salinity and major ions increased in the order Cl^- < Na^+ < total salts < $SO_4{}^{2-}$ < Ca^{2+}. The relative influence of groundwater-related factors on soil salinity decreased in the following order: groundwater depth > Na^+ > Cl^- > groundwater salinity > Ca^{2+} > $SO_4{}^{2-}$ > Mg^{2+} > $HCO_3{}^-$ > K^+ > $CO_3{}^{2-}$. Overall, the critical groundwater depths and dominant controlling factors identified in this study provide a scientific basis for mitigating soil salinization through groundwater regulation in similar irrigation districts.

Author Contributions: Conceptualization, Y.B.; Methodology, M.Z. and Z.C.; Formal analysis, W.Z.; Investigation, B.C., B.D. and J.X.; Writing—original draft, Z.S.; Writing—review & editing, Z.S., Y.B., M.Z., W.Z., B.C., B.D., J.X. and Z.C. All authors have read and agreed to the published version of the manuscript.

Funding: This research was funded by the Region "Tianshan Elite" Science and Technology Innovation Leading Talent Project (2024TSYCLJ0024) and Autonomous Major Science and Technology Special Projects in Autonomous Region (2023A02012-1, 2023A02002-4).

Data Availability Statement: The original contributions presented in this study are included in the article. Further inquiries can be directed to the corresponding authors.

Conflicts of Interest: The authors declare no conflicts of interest.

Abbreviations

The following abbreviations are used in this manuscript:

TDS Total Dissolved Solids

References

1. Wang, J.; Ding, J.; Wang, Y.; Ge, X.; Lizaga, I.; Chen, X. Soil Salinization in Drylands: Measure, Monitor, and Manage. *Ecol. Indic.* **2025**, *175*, 113608. [CrossRef]
2. Sahab, S.; Suhani, I.; Srivastava, V.; Chauhan, P.S.; Singh, R.P.; Prasad, V. Potential Risk Assessment of Soil Salinity to Agroecosystem Sustainability: Current Status and Management Strategies. *Sci. Total Environ.* **2021**, *764*, 144164. [CrossRef] [PubMed]
3. Tarolli, P.; Luo, J.; Park, E.; Barcaccia, G.; Masin, R. Soil Salinization in Agriculture: Mitigation and Adaptation Strategies Combining Nature-Based Solutions and Bioengineering. *iScience* **2024**, *27*, 108830. [CrossRef] [PubMed]
4. Ge, X.; Ding, J.; Amantai, N.; Xiong, J.; Wang, J. Responses of Vegetation Cover to Hydro-Climatic Variations in Bosten Lake Watershed, NW China. *Front. Plant Sci.* **2024**, *15*, 1323445. [CrossRef]
5. Niu, X.X.; Gao, S.S.; Li, W.C.; Jia, Z.J.; Wu, Y.Y.; Chen, J.H.; Ma, D.X. Research Progress and Prospects on Impacts of Groundwater Dynamics on Soil Water and Salt Based on Bibliometrics. *Bull. Soil Water Conserv.* **2024**, *44*, 122–133. [CrossRef]
6. Guan, X.Y.; Wang, S.L.; Gao, Z.Y.; Lv, Y.; Fu, X.J. Spatio-Temporal Variability of Soil Salinity and Its Relationship with the Depth to Groundwater in Salinization Irrigation District. *Acta Ecol. Sin.* **2012**, *32*, 1202–1210. [CrossRef]
7. Akramkhanov, A.; Martius, C.; Park, S.J.; Hendrickx, J.M.H. Environmental Factors of Spatial Distribution of Soil Salinity on Flat Irrigated Terrain. *Geoderma* **2011**, *163*, 55–62. [CrossRef]
8. Jia, H.; Li, B.Z.; Li, W.H. Water and Salt Transport Simulation under Irrigation and Drainage Combination Based on HYDRUS-1D Model. *Water Sav. Irrig.* **2021**, *1*, 27–32.
9. Chen, Z.; Han, S.; Li, H.; Yuan, R.; Yang, Y.; Yang, Y.; Wang, J.; Jiang, Y. Agricultural Development Characteristics and Irrigation Efficiency Evaluation in the Yarkant River Basin Irrigation District. *Chin. J. Eco-Agric.* **2025**, *33*, 1261–1274. [CrossRef]
10. Cai, S.J. Research on the Dynamics of Water and Salt in Farmland and the Regulation of Irrigation and Drainage in Karamay Agricultural Comprehensive Development Zone. Master's Thesis, Xinjiang Agricultural University, Urumqi, China, 2025.
11. Tavakoli-Kivi, S.; Bailey, R.T.; Gates, T.K. A Salinity Reactive Transport and Equilibrium Chemistry Model for Regional-Scale Agricultural Groundwater Systems. *J. Hydrol.* **2019**, *572*, 274–293. [CrossRef]
12. Sahoo, M.; Das, T.; Kumari, K.; Dhar, A. Space–Time Forecasting of Groundwater Level Using a Hybrid Soft Computing Model. *Hydrol. Sci. J.* **2017**, *62*, 561–574. [CrossRef]
13. Breiman, L. Random Forests. *Mach. Learn.* **2001**, *45*, 5–32. [CrossRef]
14. Li, B.; Yang, G.; Wan, R.; Dai, X.; Zhang, Y. Comparison of Random Forests and Other Statistical Methods for the Prediction of Lake Water Level: A Case Study of the Poyang Lake in China. *Hydrol. Res.* **2016**, *47*, 69–83. [CrossRef]
15. Lei, G.; Zeng, W.; Yu, J.; Huang, J. A Comparison of Physical-Based and Machine Learning Modeling for Soil Salt Dynamics in Crop Fields. *Agric. Water Manag.* **2023**, *277*, 108115. [CrossRef]
16. Xiong, J.; Ge, X.; Ding, J.; Wang, J.; Zhang, Z.; Zhu, C.; Han, L.; Wang, J. Optimal Time-Window for Assessing Soil Salinity via Sentinel-2 Multitemporal Synthetic Data in the Arid Agricultural Regions of China. *Ecol. Indic.* **2025**, *176*, 113642. [CrossRef]
17. Zhao, Y.; Miao, Q.; Shi, H.; Li, X.; Yan, J.; Yang, S.; Hou, C.; Yu, C.; Feng, W.; Hao, J. Inversion of Soil Salinization at the Branch Canal Scale in the Hetao Irrigation District Based on Improved Spectral Indices. *Agric. Water Manag.* **2025**, *316*, 109608. [CrossRef]
18. Bao, S.D. *Soil Agrochemical Analysis*; China Agricultural Press: Beijing, China, 2000.
19. Liang, F.; Li, Z.Q.; Zhang, L. *Practical Q&A and Case Analysis on Saline-Alkali Land Improvement Technology*; China Agricultural Press: Beijing, China, 2018.
20. Liu, G.; Tian, C.; Mai, W.; Azeem, A.; Yang, J. Spatial and Temporal Variation in Soil Salinity and Correlation with Groundwater Depth in the Karamay Irrigation District of China. *Sustainability* **2023**, *15*, 15680. [CrossRef]
21. Ren, J.; Guo, T.; Tian, C.; Mai, W.; Mao, X. Modeling Water and Salt Migration in Groundwater and Vadose Zones to Assess Agricultural Sustainability in Karamay Irrigation District. *Agric. Water Manag.* **2025**, *317*, 109611. [CrossRef]

22. Liu, Q.; Hanati, G.; Danierhan, S.; Liu, G.; Zhang, Y.; Zhang, Z. Identifying Seasonal Accumulation of Soil Salinity with Three-Dimensional Mapping—A Case Study in Cold and Semiarid Irrigated Fields. *Sustainability* **2020**, *12*, 6645. [CrossRef]
23. Liu, J.; Huang, Q.; Li, Z.; Liu, N.; Li, J.; Huang, G. Effect of Autumn Irrigation on Salt Leaching under Subsurface Drainage in an Arid Irrigation District. *Water* **2023**, *15*, 2296. [CrossRef]
24. Que, Z.L.; Zhuang, W.H.; Tan, B. Study on Pore Size Exclusion Effect of Colloid Release in Aquifer Driven by Salinity Gradient. *Acta Sci. Circumstantiae* **2024**, *44*, 248–254. [CrossRef]
25. Wang, D.D.; Yu, Z.T.; Cheng, M.; Zhao, C.Y.; Ding, J.L.; Zhang, X.L. Characteristics of Soil Salinity under Different Land Use Types in Weigan River Oasis. *Arid. Land Geogr.* **2018**, *41*, 349–357. [CrossRef]
26. Fu, C.; Xue, J.; Chen, J.; Cui, L.; Wang, H. Evaluating Spatial and Temporal Variations of Soil Water, Heat, and Salt under Autumn Irrigation in the Hetao Irrigation District Based on Distributed SHAW Model. *Agric. Water Manag.* **2024**, *293*, 108707. [CrossRef]
27. Cai, S.J.; Bai, Y.G.; Zhang, J.H.; Zheng, M.; Lu, Z.L.; Sun, P.; Zhao, J.H.; Yang, J.G. Seasonal variation of soil salinity and its response to groundwater under different land use patterns. *J. Agric. Resour. Environ.* **2024**, *41*, 1449–1458.
28. Hou, X.; Xiang, Y.; Fan, J.; Zhang, F.; Hu, W.; Yan, F.; Xiao, C.; Li, Y.; Cheng, H.; Li, Z. Spatial Distribution and Variability of Soil Salinity in Film-Mulched Cotton Fields under Various Drip Irrigation Regimes in Southern Xinjiang of China. *Soil Tillage Res.* **2022**, *223*, 105470. [CrossRef]
29. Wei, J.T.; Zhang, J.X.; Fan, W.B.; Xu, Z.Y.; Dong, Q.Q.; Li, C.X.; Wang, Y.Q. Effect of the Plough Bottom Depth on the Soil Water and Salt Transport under Mulched Drip Irrigation. *Chin. J. Soil Sci.* **2021**, *52*, 845–853. [CrossRef]
30. Zhao, Y.; Feng, Q.; Yang, H. Soil Salinity Distribution and Its Relationship with Soil Particle Size in the Lower Reaches of Heihe River, Northwestern China. *Environ. Earth Sci.* **2016**, *75*, 810. [CrossRef]
31. Chen, S.; Mao, X.; Shukla, M.K. Evaluating the Effects of Layered Soils on Water Flow, Solute Transport, and Crop Growth with a Coupled Agro-Eco-Hydrological Model. *J. Soils Sediments* **2020**, *20*, 3442–3458. [CrossRef]
32. Wang, R.; Xiong, L.; Xu, X.; Liu, S.; Feng, Z.; Wang, S.; Huang, Q.; Huang, G. Long-Term Responses of the Water Cycle to Climate Variability and Human Activities in a Large Arid Irrigation District with Shallow Groundwater: Insights from Agro-Hydrological Modeling. *J. Hydrol.* **2023**, *626*, 130264. [CrossRef]
33. Wang, C.; Luo, Y.; Huo, Z.; Liu, Z.; Liu, G.; Wang, S.; Lin, Y.; Wu, P. Salt Accumulation during Cropping Season in an Arid Irrigation Area with Shallow Water Table Depth: A 10-Year Regional Monitoring. *Water* **2022**, *14*, 1664. [CrossRef]
34. An, Z.; Wang, R.; Chai, M.; Li, X.; Li, W. Influence of Spring and Winter Irrigation on Salt Transport in Soil during Freeze-Thaw Cycles. *J. Hydrol.* **2025**, *663*, 134140. [CrossRef]
35. Sheikhbaglou, A.; Khodaverdiloo, H.; Zeinalzadeh, K.; Kheirfam, H.; Azad, N. Fitting Process-Dependence Performance of the van Genuchten Soil Water Retention Model to Simulate the Soil Water Flow. *Soil Tillage Res.* **2021**, *209*, 104952. [CrossRef]
36. Wang, H.; She, D.; Cardoso, R. Understanding the Effect of Seasonal Climate Variability on the Salinity in Unsaturated Agricultural Soil. *Agronomy* **2023**, *13*, 2802. [CrossRef]
37. Chen, Y.B.; Hu, S.J.; Luo, Y.; Tian, C.Y.; Yin, C.H. Relationship between Salt Accumulation in Topsoil of Deserted Land and Groundwater in Areas with Shallow Groundwater Table in Kashi, Xinjiang. *Acta Pedol. Sin.* **2014**, *51*, 75–81. [CrossRef]
38. Qi, T.; Huang, J.; Sun, Y.X.; Xu, F.; Zhang, Y.L.; Wang, J.X.; Wang, X.Y. Characteristics of Salt Ion Transport during the Period of Low Salt Area Development in Saline Soil under Drip Irrigation. *Soils Crops* **2021**, *10*, 47–59.
39. Sun, G.; Zhu, Y.; Gao, Z.; Yang, J.; Qu, Z.; Mao, W.; Wu, J. Spatiotemporal Patterns and Key Driving Factors of Soil Salinity in Dry and Wet Years in an Arid Agricultural Area with Shallow Groundwater Table. *Agriculture* **2022**, *12*, 1243. [CrossRef]
40. Amaranto, A.; Munoz-Arriola, F.; Corzo, G.; Solomatine, D.P.; Meyer, G. Semi-Seasonal Groundwater Forecast Using Multiple Data-Driven Models in an Irrigated Cropland. *J. Hydroinform.* **2018**, *20*, 1227–1246. [CrossRef]
41. Wang, G.S.; Shi, H.B.; Li, X.Y.; Guo, J.W.; Wang, W.G.; Wu, D. Estimation of Salt Transport and Relationship with Groundwater Depth in Different Land Types in Hetao Irrigation Area. *Trans. Chin. Soc. Agric. Mach.* **2020**, *51*, 255–269. [CrossRef]

Disclaimer/Publisher's Note: The statements, opinions and data contained in all publications are solely those of the individual author(s) and contributor(s) and not of MDPI and/or the editor(s). MDPI and/or the editor(s) disclaim responsibility for any injury to people or property resulting from any ideas, methods, instructions or products referred to in the content.